Experimental observation of synchronous competition in the Chua system

Zheng Le, Victor Castro, W. B. Pardo, J. A. Walkenstein, and Marco Monti
Nonlinear Dynamics Lab, University of Miami, 1320 Campo Sano Drive, Coral Gables, Florida 33146, USA

Epaminondas Rosa, Jr.
Department of Physics, Illinois State University, Normal, Illinois 61790-4560, USA

(Received 20 November 2006; revised manuscript received 21 March 2007; published 31 May 2007)

We present experimental results for two different sinusoidal functions competing to phase synchronize a Chua oscillator. Our approach involves real-time observation of the synchronization process. It shows that depending on the amplitude and frequency values of the two sinusoidal functions, the Chua oscillator can stay phase synchronized to one or the other of the inputs all the time or can alternate synchronous states between them. Numerical simulations show good agreement with the experimental observations.

DOI: 10.1103/PhysRevE.75.056216 PACS number(s): 05.45.Xt, 05.45.Gg

I. INTRODUCTION

Synchronization [1] has become a well-known and widely used feature in driven chaotic oscillators. In particular, phase synchronization, has been studied in a variety of situations, both theoretical and numerical [2] and experimental [3]. This is the case where the amplitudes of response and drive signals are disconnected, but their phases exhibit a strong correlation. More recently, numerical and experimental studies have shown that simultaneously forcing a chaotic system with two distinct periodic oscillators yields interesting response behaviors [4]. The results we present here involve the simultaneous pacing of an experimental Chua system [5] with two independent periodic oscillators. We use real-time detection techniques that prove to be useful and reliable for observing synchronous and nonsynchronous states, as well as transitions between them. Real-time detection capability becomes very convenient, for instance, for the adjustment of experimental control parameters to induce cases of interest. Numerical simulations confirm and validate the experimental results. One potential motivation for this work is the existence of a number of systems subject to simultaneous external influences, such as two neurons sending signals to another neuron. In addition, it is a first step toward more complex experimental situations where several oscillators compete for synchronization with a single nonlinear system.

II. EXPERIMENTAL SETUP

Our experimental setup is represented schematically in Fig. 1 below. The circuit is composed of two capacitors C_1 and C_2, two resistors R and r, one inductor L, and the nonlinear (piecewise linear) resistor R_{NL} [2,5]. The input $A_1 \sin(\omega_1 t)+A_2 \sin(\omega_2 t)$ can be viewed as a small perturbation, since the amplitudes A_1 and A_2 are of the order of 0.5% of the amplitude of the signal they are intended to affect. The frequencies ω_1 and ω_2 (in general $\omega_1 \neq \omega_2$) represent the perturbation frequencies. Data acquisition is performed using a PCI-MIO-16E4 National Instruments board connected to a computer controlled by software developed in LabView. The dynamical variables of interest in this circuit are the voltages V_{C1} across capacitor C_1 and V_{C2} across capacitor C_2, and the current i_L across the inductor L.

We adjust the experimental parameter values such that the V_{C2} versus V_{C1} two-dimensional projection of the attractor corresponds to a single scroll attractor moving around an unstable saddle focus. In this case a phase can readily be defined by the angle $\phi_{\mathrm{Chua}}=\tan^{-1} V_{C2}/V_{C1}$. Likewise, ϕ_1 and ϕ_2 represent the phases for the two sinusoidal signals. We say that the Chua system is in phase synchrony with the sinusoidal function 1 (2) if the phase difference $(\Delta\phi)_{1,2} = \phi_{\mathrm{Chua}} - \phi_{1,2}$ remains bounded and less than 2π. In the phase synchronous regime there are no 2π phase slips between the two oscillators. If, as time goes by, one of the oscillators (Chua or sinusoidal function) moves ahead at least one full lap with respect to the other, we say that the synchronous state has been broken. It is a transition process that may take a few cycles to be completed. After the transition, the two oscillators may get in step with each other again, over an extended time interval until another synchronization break takes place. See the second paper in Ref. [2] for more details.

III. REAL-TIME DETECTION OF PHASE SYNCHRONISM

Our goal here is to study the behavior of the Chua circuit under the action of two simultaneous sinusoidal functions. For this purpose, we cannot overemphasize the importance of real-time detection and observation of various synchronous states. A real-time picture of the full two-dimensional projection of the V_{C2} versus V_{C1} forced Chua attractor is depicted in Fig. 2(a). Due to the small amplitude of the perturbing signals, there are no noticeable differences between

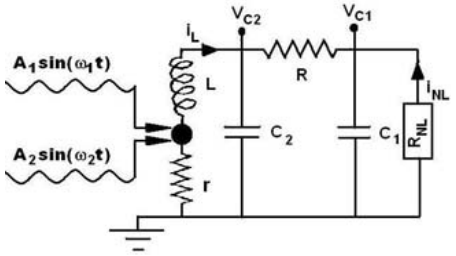

FIG. 1. The perturbed Chua circuit.

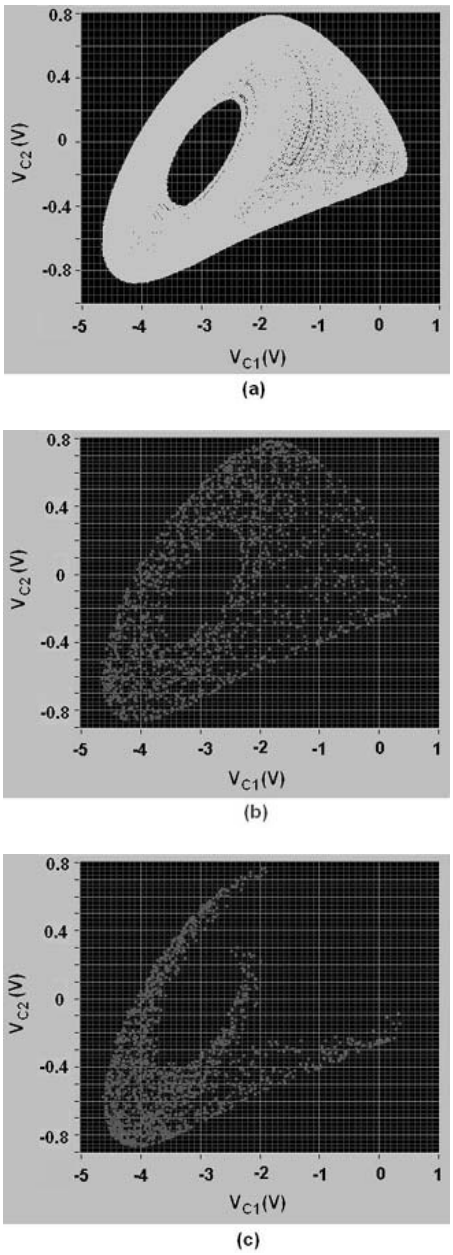

FIG. 2. Real-time computer screen frames. In (a), the full two-dimensional projection of the V_{C2} versus V_{C1} attractor is depicted. In (b) the stroboscopic map spreads all over the attractor in phase space due to lack of phase synchronism. In (c) the stroboscopic map remains constrict within a limited region of the attractor, a clear indication of phase synchronism.

the attractors of the forced and of the nonforced systems. Moreover, the effect of the two sinusoidal functions on the behavior of the system cannot be detected in real-time unless different sampling rates are used for data acquisition. Assume, for example that, under the forcing $A_1 \sin(\omega_1 t) + A_2 \sin(\omega_2 t)$, the Chua system gets in step with the sinusoidal signal $A_1 \sin(\omega_1 t)$, but not with $A_2 \sin(\omega_2 t)$. Using stroboscopic sampling of the voltages V_{C1} and V_{C2} at a rate equal to the frequency $f_2 = \omega_2 / 2\pi$ produces dots along the trajectory on the two-dimensional projection of the attractor. As depicted in Fig. 2(b), these dots are spread all over the attractor. This is so because the sinusoidal function 2 and the Chua system are not phase synchronized. However, a different picture is observed if we use an acquisition sampling rate equal to the frequency $f_1 = \omega_1 / 2\pi$. As depicted in Fig. 2(c), the dots now concentrate on a limited region of the attractor, demonstrating that the angle difference $(\Delta\phi)_1$ between the phases of the two oscillators does not grow larger than 2π. This is done in real time, as the experiment runs. The technique is applicable to chaotic systems driven by a single sinusoidal function. Its implementation is straightforward, with dependable results. It works well and is particularly useful as a first approach for checking phase synchronous states using visual inspection directly from the scope.

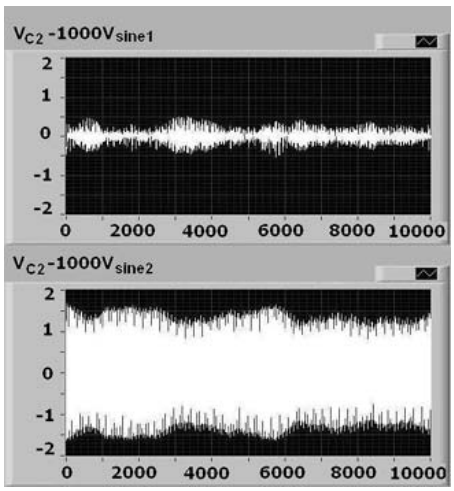

FIG. 3. Top frame: time evolution of the difference between Chua's V_{C2} and the sinusoidal signal 1. Bottom frame: time evolution of the difference between Chua's V_{C2} and the sinusoidal signal 2.

For simultaneous observation of the synchronous states between the Chua oscillator and two sinusoidal functions we may rely on a similar but different technique. It consists of plotting the difference between the signal output of the Chua system and the two sinusoidal functions, separately. Take, for example, the Chua voltage V_{C2} and the sinusoidal signal 1. Because $V_{C2} \in [-1V, +1V]$ and $V_{\sin e1} \in [-1mV, +1mV]$, we multiply the amplitude of the sinusoidal signal by a factor of 1000. As the two signals are in step with each other, their maxima match well except for small deviations, and so do their minima. In fact, some mismatch exists because the Chua signal is chaotic and the sinusoidal function is periodic. In this case their phases are in step with each other and their amplitudes are, of course, different. Sometimes the amplitude of the Chua is larger than the amplitude of the sinusoidal function, sometimes it is smaller. However, the magnitude of the difference between these two signals remains small, as depicted at the top of Fig. 3. At the bottom we plot the difference between the voltage V_{C2} and the sinusoidal signal 2 (also multiplied by a factor of 1000). Notice that now we obtain a high amplitude oscillation because in this case the two signals are not in phase synchrony.

IV. DISCUSSION

We now discuss and analyze experimental data generated and acquired with the help of the techniques described in the

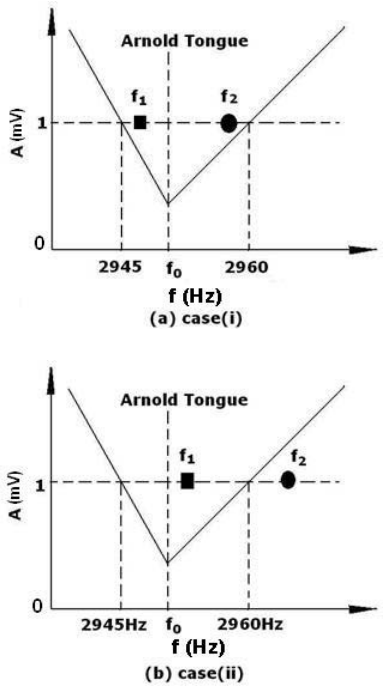

FIG. 4. Schematic representation of the parameter space A-f for the case of a single sinusoidal signal coupled to the Chua system. (a) In case (i), $f_1<f_0<f_2$, while both f_1 and f_2 are inside the synchronization tongue; (b) in case (ii), f_1 is inside the Arnold tongue while f_2 is outside the tongue.

previous section. Figures 4(a) and 4(b) illustrate schematically where the two forcing frequencies f_1 and f_2 are located with respect to the Arnold tongue for phase synchronism of a singly driven system. The chaotic Chua system in the single-scroll regime is characterized by a predominant frequency f_P, which corresponds to the frequency f_0 at the tip of the tongue. The farther the pacer signal frequency is from f_P the larger the amplitude required to achieve phase synchronism [2].

Figures 4(a) and 4(b) correspond to two cases where we analyze phase synchronous processes of the chaotic Chua oscillator simultaneously forced with two different sinusoidal functions.

Case (i). In this case, illustrated in Fig. 4(a), both signal frequencies are inside the Arnold tongue, with $f_1<f_0<f_2$. The experimental values are $A_1=A_2=1$ mV, $f_1=2947$ Hz, $f_2=2959$ Hz, $f_0=2950$ Hz. In this configuration, as the two sinusoidal driving signals compete for the attention of the Chua system, drive 1 tries to slow down the Chua oscillator and drive 2 tries to speed it up. If the Chua oscillator were separately driven by f_1 or f_2, phase synchronism would happen in both cases because both f_1 and f_2 are inside the Arnold tongue. However the simultaneous drive of the system with f_1 and f_2 yields a different result. The Chua system phase synchronizes with one of the forcing signals for a while, then breaks it and phase synchronizes with the other forcing signal for a while, breaks it and goes back phase synchronizing again with the previous one, etc. This behavior can be observed by plotting the phase difference (versus time) between the Chua and the two drives, shown in Figs.

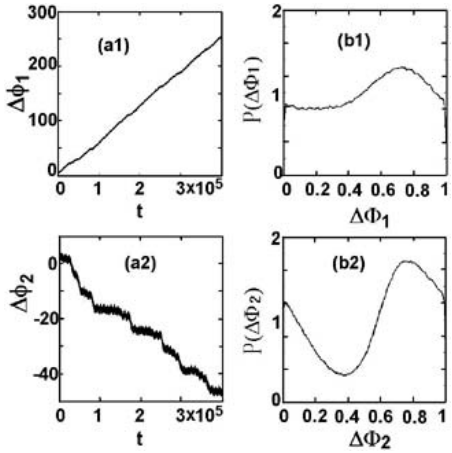

FIG. 5. Phase difference (versus time) between Chua and drive 1 (a1) and between Chua and drive 2 (a2). Histograms approximations of the distribution functions $P(\Delta\Phi_{1,2})$, where $\Delta\Phi_{1,2}=[\Delta\phi_{1,2}/(2\pi)]$ modulo 1, are shown in (b1) and (b2).

5(a1) and 5(a2). In Fig. 5(a1) we see that the graph of $\Delta\phi_1$ versus t consists of an approximate linear increase except for very small plateaus, while in Fig. 5(a2), longer plateaus point out longer time intervals of phase locking of ϕ_{Chua} to ϕ_2. This indicates that the Chua favors longer synchronous states with drive 2. The steps between plateaus observed more clearly in Fig. 5(a2) correspond to phase slips of 2π where drive 2 moves one full lap ahead of the Chua oscillator. It is a transition between two consecutive synchronous states and may take a few cycles to be completed. A close look into Figs. 5(a1) and 5(a2) reveals that the phase slips in one of them correspond to plateaus in the other and vice versa, demonstrating that in this case, the Chua oscillator phase synchronizes with only one of the drives at a time. It alternates synchronous states between the two drives, jumping back and forth at irregular time intervals. Notice that even though $f_1=2947$ Hz is closer to $f_0=2950$ Hz than $f_2=2959$ Hz, the Chua oscillator synchronizes better with f_2 than with f_1. This is due to the higher frequency with which the sinusoidal function 2 hits the Chua system making it more prone to stay in sync with driver 2 as opposed to driver 1. As we shall see, this is also the case for numerical simulations of a similar setup. Figures 5(b1) and 5(b2) display histograms approximations of the distribution functions $P(\Delta\Phi_{1,2})$, where $\Delta\Phi_{1,2}=[\Delta\phi_{1,2}/(2\pi)]$ modulo 1. The histograms are clear indication that there exist statistically significant correlations between ϕ_{Chua} and $\phi_{1,2}$. Weak as the connection may be, each of the phases ϕ_1 and ϕ_2 synchronizes to the phase of the chaotic Chua in an alternating manner.

Figures 6(a) and 6(b) show stroboscopic surfaces of section of the Chua trajectory at the frequencies f_1 and f_2, respectively. For each point on a long trajectory we plot r versus $[\phi \text{ modulo } 2\pi]/\omega_{1,2}-t$, where $r=\sqrt{(V_{C1})^2+(V_{C2})^2}$ is the radius of the two-dimensional projection of the Chua attractor. This provides a polar coordinates picture of the density of points strobed on the attractor. Regions of high density of points in the top picture correspond to regions of low density of points in the bottom picture, and vice versa. This is as expected because the Chua oscillator synchronizes

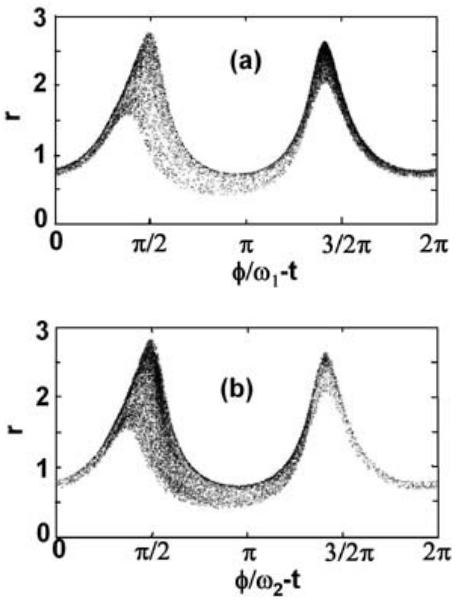

FIG. 6. Stroboscopic surfaces of section of the experimental Chua (perturbed trajectory) sampled at frequencies (a) f_1 and (b) f_2.

to each drive in an alternating manner. That is, the Chua oscillator synchronizes to drive 1 while losing synchrony with drive 2, and vice versa. Figures 6 show many pairs of 2π cycles folded on top of each other (mod 2π) because we wanted to depict more clearly the difference between the low and high density regions. Of course, the pattern continues indefinitely on either direction of the figures. High density regions correspond to places where the trajectory stays over long time intervals [plateaus in Figs. 5(a1) and 5(a2)].

The low-density regions are regions that the orbit traverses relatively faster (steps), while the high-density regions correspond to regions where the orbits stay longer (plateaus). Therefore, when Fig. 6(a) has a low-density region, Fig. 6(b) has a high-density region.

Figure 7 displays $\Delta\phi_2$ versus $\Delta\phi_1$. The staircaselike structure shows that when $\Delta\phi_1$ varies over time, $\Delta\phi_2$ is approximately constant and vice versa; the approximately horizontal portions of the graph correspond to plateaus of $\Delta\phi_1$ and the approximately vertical portions correspond to plateaus of $\Delta\phi_2$. This reassures the idea of the chaotic oscillator switching back and forth its synchronous state with the phases $\phi_{1,2}$ of the competing signals.

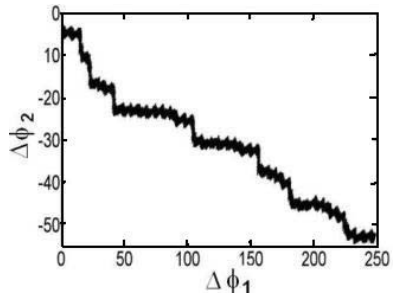

FIG. 7. $\Delta\phi_2$ versus $\Delta\phi_1$. The staircaselike structure indicates that there are alternating time intervals in which ϕ is locked to either ϕ_1 or to ϕ_2.

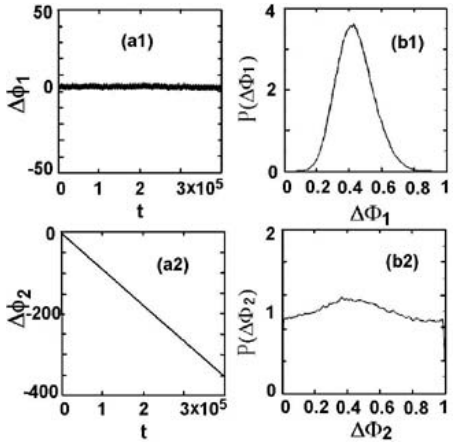

FIG. 8. Phase difference (versus time) between Chua and drive 1 (a1) and between Chua and drive 2 (a2). Histograms approximations of the distribution functions $P(\Delta\Phi_{1,2})$, where $\Delta\Phi_{1,2}=[\Delta\phi_{1,2}/(2\pi)]$ modulo 1, are shown in (b1) and (b2).

Case (ii). In this case, illustrated in Fig. 4(b), one sinusoidal signal frequency (signal 1) is phase synchronized (lies inside the Arnold tongue) with the Chua attractor, while the other signal is unsynchronized (outside the Arnold tongue) with the Chua attractor. The experimental values are $A_1=A_2=1$ mV, $f_1=2951.5$ Hz, $f_2=2965.5$ Hz, $f_0=2950$ Hz. In Fig. 8(a1) the phase difference between the chaotic oscillator and drive 1 remains bounded and does not increase (or decrease). There are no 2π phase slips and the two oscillators remain with their phases in step with each other continuously. On the other hand, the phase difference between the chaotic attractor and drive 2 seems to decrease continuously in a linear manner. These continuous states of synchrony with one drive and nonsynchrony with the other is further illustrated with the histogram approximations of the probability distributions of $\Delta\Phi_{1,2}=[\Delta\phi_{1,2}/(2\pi)]$ modulo 1 shown in Figs. 8(b1) and 8(b2). As we can see, the histogram for the synchronous state presents a sharp peak [Fig. 8(b1)], while the corresponding histogram for the nonsynchronous state is almost flat [Fig. 8(b2)].

The corresponding stroboscopic surfaces of section are shown, respectively, in Figs. 9(a) and 9(b). Notice in Fig. 9(a) the bounded region containing the surface of section points for the continuous synchronous state. In Fig. 9(b) the density of points is evenly distributed over the 2π angle range. This indicates a continuous phase slip between the phase of the chaotic Chua and the phase of the sinusoidal pacer 2.

V. NUMERICAL SIMULATION

Numerical results obtained from model equations for the Chua system [2] forced with two sinusoidal functions show very good agreement with the experimental measurements. The state equations for the system, with the two pacing functions $A_1\sin(\psi_1 t)$ and $A_2\sin(2t)$, are as follows:

$$C_1\frac{dx}{dt}=\frac{(y-x)}{R}-g(x),$$

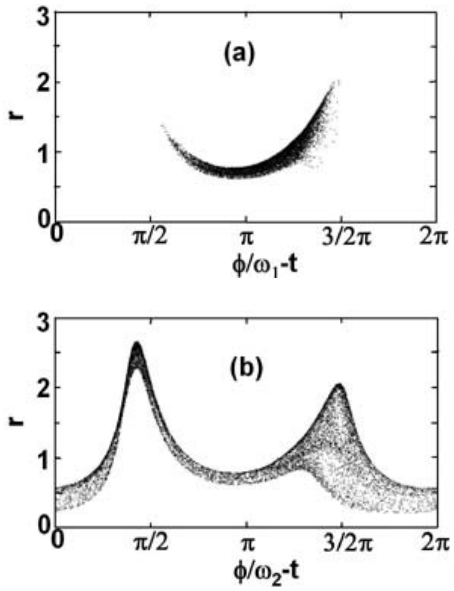

FIG. 9. Stroboscopic surfaces of section of the Chua perturbed trajectory at frequencies (a) f_1 (inside the tongue) and (b) f_2 (outside the tongue).

$$C_2\frac{dy}{dt} = \frac{(x-y)}{R} + z,$$

$$-L\frac{dz}{dt} = y + A_1\sin(\omega_1 t) + A_2\sin(\omega_2 t), \tag{1}$$

where $g(x)$ is a piecewise-linear function defined by

$$g(x) = m_0 x + 0.5(m_1 - m_0)(|x + B_p| - |x - B_p|). \tag{2}$$

Here, C_1 and C_2 are the capacitances of the two capacitors, L is the inductance of inductor, R is the resistance of the linear resistor. The relation of $g(x)$ is shown graphically in Fig. 10.

The slopes in the inner and outer regions are m_0 and m_1, respectively; $\pm B_P$ denote the breakpoints. In Equations (1) x and y are the voltage across the capacitors C_1 and C_2, respectively, and z is the electric current across the inductor L. The parameters used in the numerical simulation of the circuit are $C_1=0.1$, $C_2=1.0$, $L=0.163$, $R=1.73$, $m_0=-0.5$, $m_1=-0.8$, and $B_P=1.0$.

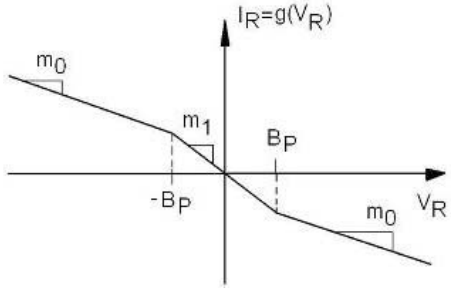

FIG. 10. Three-segment piecewise-linear v-i characteristic of the nonlinear resistor in Chua's circuit. The outer regions have slopes m_0; the inner region has slope m_1. There are two breakpoints at $\pm B_P$.

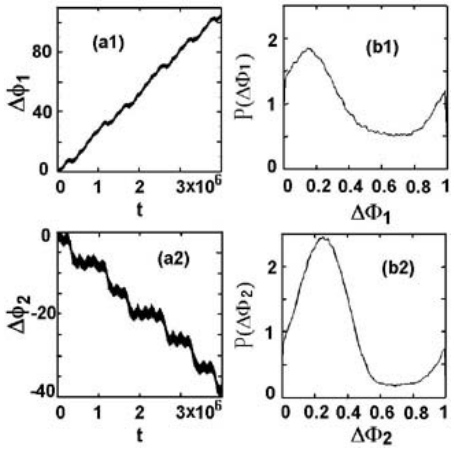

FIG. 11. Phase difference (versus time) between Chua and drive 1 (a1) and between Chua and drive 2 (a2). Histograms approximations of the distribution functions $P(\Delta\Phi_{1,2})$, where $\Delta\Phi_{1,2}=[\Delta\phi_{1,2}/(2\pi)]$ modulo 1, are shown in (b1) and (b2).

As we did before with the experimental setup, we consider two different choices of frequency values f_1 and f_2 with two equal amplitudes $A_1=A_2$. Here, we use $A_{1,2}\ll 1$, $\omega_{1,2}$ close to ω_{peak}. As before, two cases are analyzed.

Case (i). In this case, both signal frequencies are inside the Arnold tongue (the tongue of phase synchronism for a single driving signal). $A_1=A_2=2.5\times10^{-3}$, $f_1=0.1423$, $f_2=0.1429$, $f_0=0.1425$. Figures 10 show the reaction of the chaotic Chua in terms of synchronizing with one or the other forcing sinusoidal functions. In Figs. 11(a1) and 11(a2) we see the alternating synchronous effect whereby plateaus in Fig. 11(a1) correspond to phase slips in Fig. 11(a2) and vice versa. Here also, as was the case in the experimental implementation, the Chua oscillator favors synchrony with driver $f_2=0.1429$, even though driver $f_1=0.1423$ is closer to $f_0=0.1425$. However driver f_2 hits the Chua system more often

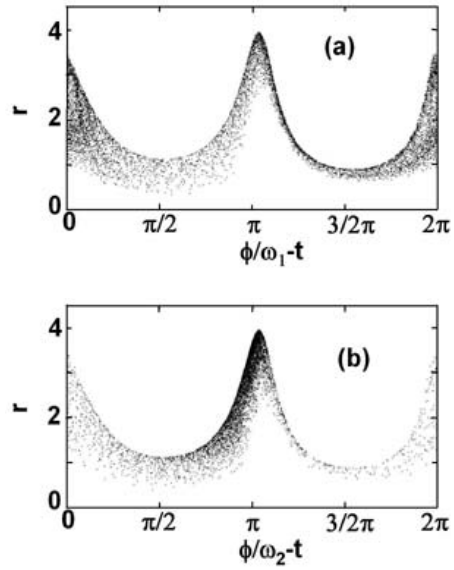

FIG. 12. Stroboscopic surfaces of section of the numerical Chua (perturbed trajectory) sampled at frequencies (a) f_1 and (b) f_2.

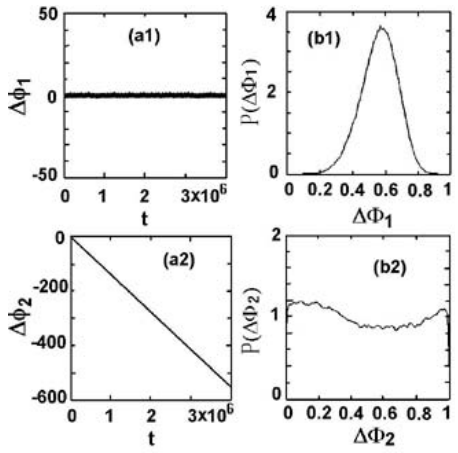

FIG. 13. Phase difference (versus time) between Chua and drive 1 (a1) and between Chua and drive 2 (a2). Histograms approximations of the distribution functions $P(\Delta\Phi_{1,2})$, where $\Delta\Phi_{1,2}=[\Delta\phi_{1,2}/(2\pi)]$ modulo 1, are shown in (b1) and (b2).

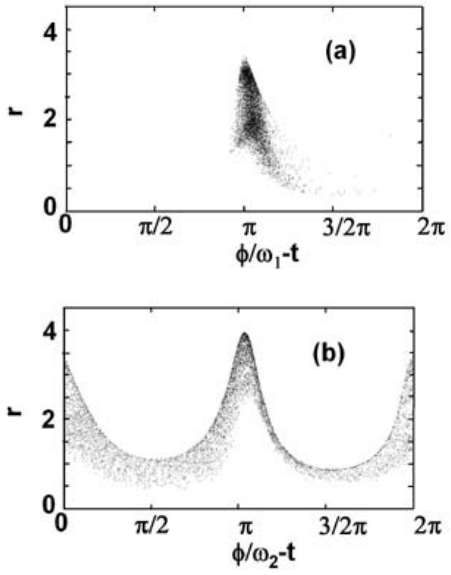

FIG. 14. Stroboscopic surfaces of section of the Chua perturbed trajectory at frequencies (a) f_1 (inside the tongue) and (b) f_2 (outside the tongue).

than driver f_1, therefore exerting a larger influence on the system. The histogram approximations of the probability distributions are depicted in Figs. 11(b1) and 11(b2). Figures 12(a) and 12(b) show stroboscopic surfaces of section for both sinusoidal drives. As before, alternating regions of high density (plateaus) and low density (phase slips) of points indicate the alternating synchrony of ϕ between ϕ_1 and ϕ_2.

Case (ii). In this case, the sinusoidal signal 2 is phase synchronized (lies inside the Arnold tongue) with the Chua attractor, while the other signal (1) is unsynchronized (outside the Arnold tongue) with the Chua attractor. $A_1=A_2=2.5\times10^{-3}$, $f_1=0.1424$, $f_2=0.1445$, $f_0=0.1425$. In Fig. 12(a1), we see a constant decrease in the phase difference $\Delta\phi_2$, which represents phase unlocking. In Fig. 13(a1), we see that the value of $\Delta\phi_1$ versus time remains small and stable over time. Approximations of the corresponding probability distributions are shown in Figs. 13(b1) and 13(b2). As we can see, Fig. 13(b2) is almost flat, which indicates phase locking between ϕ to ϕ_1. The long plateau seen in Fig. 13(a1) corresponds to regions of high density of points in Fig. 14(a).

Figure 14(a) shows the bounded spread of points over a modulus 2π repeat pattern. The continuous slipping of phases between ϕ to ϕ_2 is represented in Fig. 14(b) with the continuous flow of stroboscopic point over the extension of 2π but, of course, it continues spreading beyond it.

VI. FINAL REMARKS

We presented experimental and numerical results of phase synchronous states for a chaotic Chua system forced simultaneously with two different sinusoidal functions. Experimental real-time capability for visualizing the state of the system plays an important role for the choice of parameter values for data acquisition. Two particular cases were studied to illustrate the procedure. Numerical simulations outputs concur well with the experimental measurements. In one case the chaotic oscillator alternates synchronous states between the two sinusoidal functions. In the other case, the chaotic oscillator stays synchronized with one of the oscillators only. This study opens the possibility for real-time observation of experimental complex processes in which competition for phase synchronization takes place.

[1] A. Pikovsky, M. Rosenblum, and J. Kurths, *Synchronization: A Universal Concept in Nonlinear Science* (Cambridge University Press, Cambridge, 2003).

[2] M. G. Rosenblum, A. S. Pikovsky, and J. Kurths, Phys. Rev. Lett. **76**, 1804 (1996); E. Rosa, Jr., E. Ott, and M. H. Hess, *ibid.* **80**, 1642 (1998); L. Junge and U. Parlitz, Phys. Rev. E **62**, 438 (2000); G. Hu, Y. Zhang, H. A. Cerdeira, and S. Chen, Phys. Rev. Lett. **85**, 3377 (2000); D. L. Valladares, S. Boccaletti, F. Feudel, and J. Kurths, Phys. Rev. E **65**, 055208(R) (2002); R. L. Viana, C. Grebogi, S. E. de S. Pinto, S. R. Lopes, A. M. Batista, and J. Kurths, *ibid.* **68**, 067204 (2003); M. S. Baptista, S. Boccaletti, K. Josic, and I. Leyva, *ibid.* **69**, 056228 (2004); J. Gao and Z. G. Zheng, Int. J. Mod. Phys. B **18**, 2945 (2004); M. A. Zaks and E.-H. Park, Phys. Rev. E **72**, 026215 (2005); Y.-C. Lai, M. G. Frei, and Ivan Osorio, *ibid.* **73**, 026214 (2006).

[3] A. Neiman, X. Pei, D. Russell, W. Wojtenek, L. Wilkens, F. Moss, H. A. Braun, M. T. Huber, and K. Voigt, Phys. Rev. Lett. **82**, 660 (1999); C. M. Ticos, E. Rosa, Jr., W. B. Pardo, J. A. Walkenstein, and M. Monti, *ibid.* **85**, 2929 (2000); I. Z. Kiss and J. L. Hudson, Phys. Rev. E **64**, 046215 (2001); D. J. DeShazer, R. Breban, E. Ott, and R. Roy, Phys. Rev. Lett. **87**,

044101 (2001); R. Herrero, M. Figueras, F. Pi, and G. Orriols, Phys. Rev. E **66**, 036223 (2002); M. S. Baptista, T. P. Silva, J. C. Sartorelli, I. L. Caldas, and E. Rosa, *ibid.* **67**, 056212 (2003); I. Tokuda, J. Kurths, E. Allaria, R. Meucci, S. Boccaletti, and F. T. Arecchi, *ibid.* **70**, 035204(R) (2004).

[4] R. Breban and E. Ott, Phys. Rev. E **65**, 056219 (2002); R. McAllister, R. Meucci, D. DeShazer, and R. Roy, *ibid.* **67**, 015202(R) (2003); I. Leyva, E. Allaria, S. Boccaletti, and F. T. Arecchi, *ibid.* **68**, 066209 (2003); J. Gao and Z. G. Zheng, Int. J. Mod. Phys. B **18**, 2945 (2004); F. C. Meinecke, A. Ziehe, J. Kurths, and K.-R. Mueller, Phys. Rev. Lett. **94**, 084102 (2005).

[5] M. P. Kennedy, Frequenz **46**, 66 (1992).